# Dual-Readout Calorimetry
# for High-Quality Energy Measurements

*Progress Report*

*Presented by:*

Dr. Richard Wigmans[1]

*on behalf of the RD52 (DREAM) Collaboration*

4 April 2017

[1]Contact person. Tel. [806] 834 6283, FAX [806] 742 1182, E-mail: wigmans@ttu.edu

# 1  Introduction

On August 31, 2011, the CERN Research Board decided to accept the DREAM Collaboration's detector R&D proposal [1] and included it as project RD52 in its official scientific program. This document constitutes the fifth RD52 progress report. In this report, we describe our activities since the last time we reported to the SPS Committee (April 19, 2016 [2]), as well as our future plans.

Since our last report to the SPSC, one new paper with results from our 2014 test beam campaign was published. We have finalized the analyses of the hadron measurements done in October 2015. Some preliminary results of this work were shown in last year's SPSC meeting. A large paper summarizing all the analyses and their results has recently been submitted to NIM. Some highlights are presented in the next section.

In October 2016, we were granted one week of test beam in H8. We used this opportunity to test a completely new type of readout for our calorimeters, based on silicon photomultipliers (SiPM). Some of the results of this tests are shown in this report. The success of this test has encouraged us to further exploit this option. It has also drawn the attention of people who are designing experiments for future colliders, and has led to renewed interest (and funding possibilities) for the work carried out in the context of the RD52 project.

We have also made progress in constructing copper absorber structures with the required degree of precision. Two new modules, built in Ames Iowa, will soon be shipped to CERN in order to be tested there in a new round of experimental data taking. Our plans also include tests of a second-generation SiPM-equipped dual-readout calorimeter module.

In the past year, the latest RD52 results have been presented at a number of colloquia and seminars. They were also featured at the CALOR conference in May 2016, in Daegu, Korea. The talks, as well as all publications in the context of this project, can be found at the RD52 website:

*http://highenergy.phys.ttu.edu/dream/results/talks/talks.html*

Details about our various past, current and planned activities are given in the next sections.

# 2  New results

The results of our beam tests in 2014 have been summarized in the following publication:

- *New Results from the RD52 Project*,
  R. Wigmans, Nucl. Instr. and Meth. **A824** (2016) 721.

The results of our 2015 beam tests are described in the following paper:

- *Hadron detection with a dual-readout fiber calorimeter*,
  S. Lee *et al.*, submitted to Nucl. Instr. and Meth. (2017)

Some preliminary results of this work were already shown in last year's presentation. Highlights are presented in the following subsection.

## 2.1 Hadron detection with a dual-readout fiber calorimeter

### 2.1.1 Dual-readout calorimetry

The Dual-Readout approach for measuring hadron showers exploits the fact that the energy carried by the non-em shower component of hadron showers is mostly deposited by non-relativistic shower particles (protons), and therefore does not contribute to the signals of a Čerenkov calorimeter. By measuring simultaneously the visible deposited energy ($dE/dx$) and the Čerenkov light generated in the shower absorption process, one can determine $f_{\mathrm{em}}$ *event by event* and thus eliminate (the effects of) its fluctuations. The correct hadron energy can be determined from a combination of both signals.

This principle was first experimentally demonstrated by the DREAM Collaboration [3], with a Cu/fiber calorimeter. Scintillating fibers measured $dE/dx$, quartz fibers the Čerenkov light. The response ratio of these two signals was related to $f_{\mathrm{em}}$ as

$$\frac{C}{S} = \frac{f_{\mathrm{em}} + 0.21\,(1 - f_{\mathrm{em}})}{f_{\mathrm{em}} + 0.77\,(1 - f_{\mathrm{em}})} \tag{1}$$

where 0.21 and 0.77 represent the $h/e$ ratios of the Čerenkov and scintillator calorimeter structures, respectively. The hadron energy could be derived directly from the two signals [4]:

$$E = \frac{S - \chi C}{1 - \chi}, \quad \text{with} \quad \chi = \frac{\left[1 - (h/e)_S\right]}{\left[1 - (h/e)_C\right]} \approx 0.3 \tag{2}$$

The $e/h$ values, and thus the value of the parameter $\chi$ are a bit different when lead absorber is used.

In this section, we present results on the energy resolution measured for single hadrons of different energies. For the positive polarity, separate samples of protons and pions were used. No attempts were made to isolate the kaons, whose showers should also be different from pion ones in terms of the em shower component. Strangeness conservation prevents the production of leading $\pi^0$s in kaon induced showers, and therefore the characteristics of the em shower component (average value, event-to-event fluctuations in $f_{\mathrm{em}}$) are probably similar to those in proton induced showers.

For every event, two signals were available, a Čerenkov signal and a scintillation signal. The particle energy was found by combining these signals as in Equation 2, using a parameter value $\chi = 0.45$. This value is somewhat larger than for the copper based DREAM calorimeter, since the $e/h$ values for lead are somewhat smaller, both for the scintillation and the Čerenkov sampling structure [5]. We have used a value $\chi = 0.45$ for our lead based calorimeter throughout this analysis. The same procedure was used to obtain signal distributions for pions and protons over the entire energy range studied here.

The results of this study are summarized in Figure 1. Figure 1a shows the average signal per unit deposited energy (*i.e.* the *calorimeter response*) as a function of energy, for pions with energies ranging from 20 to 125 GeV. Results are given separately for the Čerenkov signals and for the dual-readout signals. Whereas the Čerenkov response increased by more than 50% over
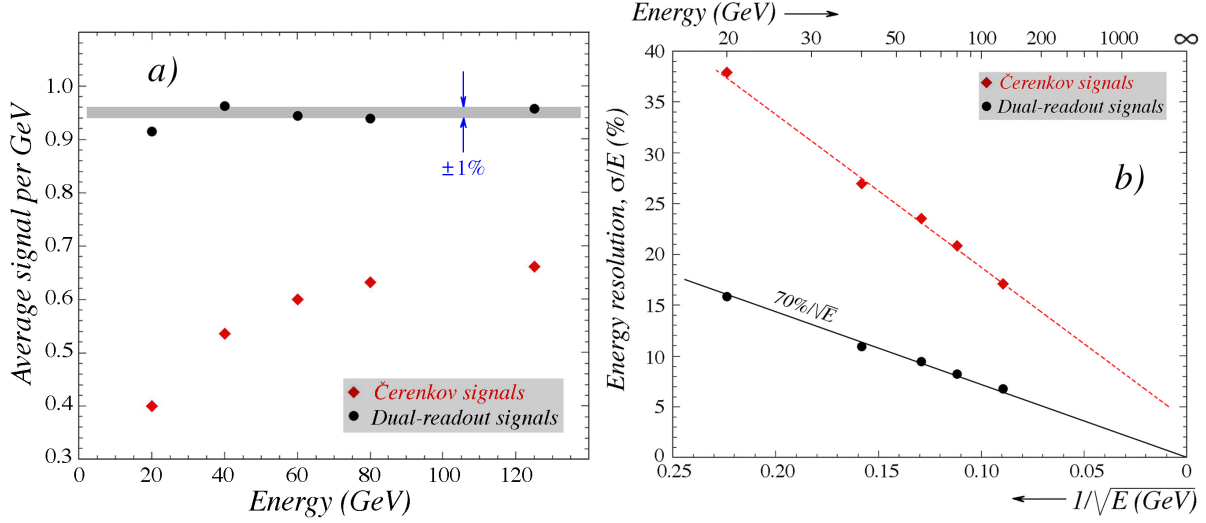
Figure 1: The hadronic response of the RD52 lead-fiber dual-readout calorimeter, for single pions. Shown are the average Čerenkov signal and the dual-readout signal (Eq. 2) per unit deposited energy, as a function of the pion energy (*a*). The hadronic energy resolution of the RD52 lead-fiber dual-readout calorimeter, for single pions. Shown are the results for the Čerenkov signals alone, and for the the dual-readout signals, obtained with Eq. 2 (*b*).

this energy range, the dual-readout response was constant to within a few percent, except for the lowest energy. The results for protons were essentially the same.

The hadronic energy resolution is shown as a function of energy in Figure 1b. The energy scale is proportional to $-E^{-1/2}$, which means that the data points should be located on a straight line through the bottom right corner of this plot if the resolution is only determined by fluctuations that are governed by Poisson statistics. Any deviation from such a line means that non-stochastic effects play a significant role. The experimental data show that the energy resolution for pions is well described by *stochastic fluctuations alone* when the dual-readout signals are considered. On the other hand, the energy resolution measured on the basis of the Čerenkov signals exhibits substantial deviations from $E^{-1/2}$ scaling. The straight line fit through the experimental data points suggests a 5% resolution at infinite energy. This is a consequence of the fact that the event-to-event fluctuations in the em shower fraction ($f_{\text{em}}$) are not stochastic.

### 2.1.2 The rotation method

Typically, measurements of the energy resolution of a calorimeter are performed with a test beam of mono-energetic particles. The width of the signal distribution of these particles is interpreted as the energy resolution of the detector. We have used this procedure as an alternative method to the standard Dual-Readout one, where the reconstructed energy of an event is compared with its true energy. In this alternative approach, we make use of the fact that we are dealing with an ensemble of monoenergetic particles of a particular type (pions, protons), but no other information about these particles, such as the value of their energy, is used.

Figure 2a shows a scatter plot of the Čerenkov signals *vs.* the scintillation signals measured with this detector for 60 GeV pions. The signals from the leakage counters were added to those

from the scintillating fibers, using the fact that the measured shower profile indicated that the side leakage at this energy was, on average, 6.4%. The energy scale for both the Čerenkov and the scintillation signals is given in units of GeV, derived from the calibration of these signals with electron showers.
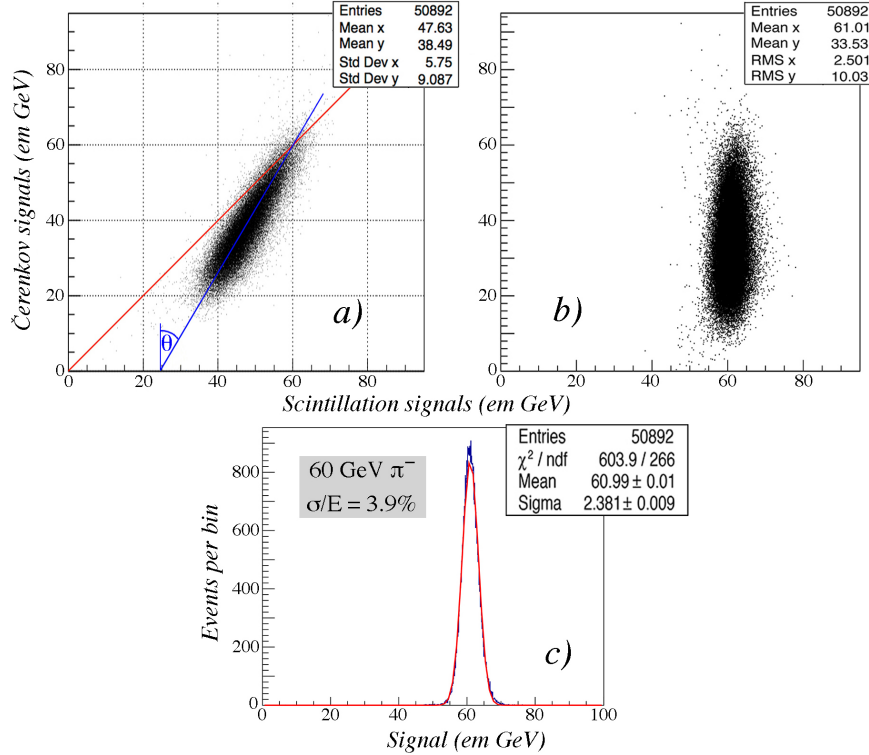


Figure 2: Signal distributions of the RD52 Dual-Readout lead/fiber calorimeter for 60 GeV pions. Scatter plot of the two types of signals as recorded for these particles ($a$) and rotated around the point where the two lines from diagram $a$ intersect ($b$). Projection of the latter scatter plot on the $x$-axis ($c$).

This scatter plot shows the data points located on a locus, clustered around a line that intersects the $C/S = 1$ line at the beam energy of 60 GeV. This is of course to be expected. In first approximation, the Čerenkov fibers only produced signals generated by the electromagnetic components of the hadron showers, predominantly $\pi^0$s. The larger the em shower fraction, the larger the $C/S$ signal ratio. Events in which (almost) the entire hadronic energy was deposited in the form of em shower components thus produced signals that were very similar to those from 60 GeV electrons and are, therefore, represented by data points located near (60,60) in this scatter plot.

We can now rotate the scatter plot over the angle $\theta$ around this intersection point and the result is shown in Figure 2b. The projection of this rotated scatter plot on the $x$-axis is shown in Figure 2c. This signal distribution is well described by a Gaussian function with a central value of 61.0 GeV and a relative width, $\sigma/E$, of 3.9%. This corresponds to $30\%/\sqrt{E}$. The narrowness of this distribution reflects the clustering of the data points around the axis of the locus in Figure 2a.

We have repeated the same procedure for data taken at +125 GeV, +80 GeV, +40 GeV and
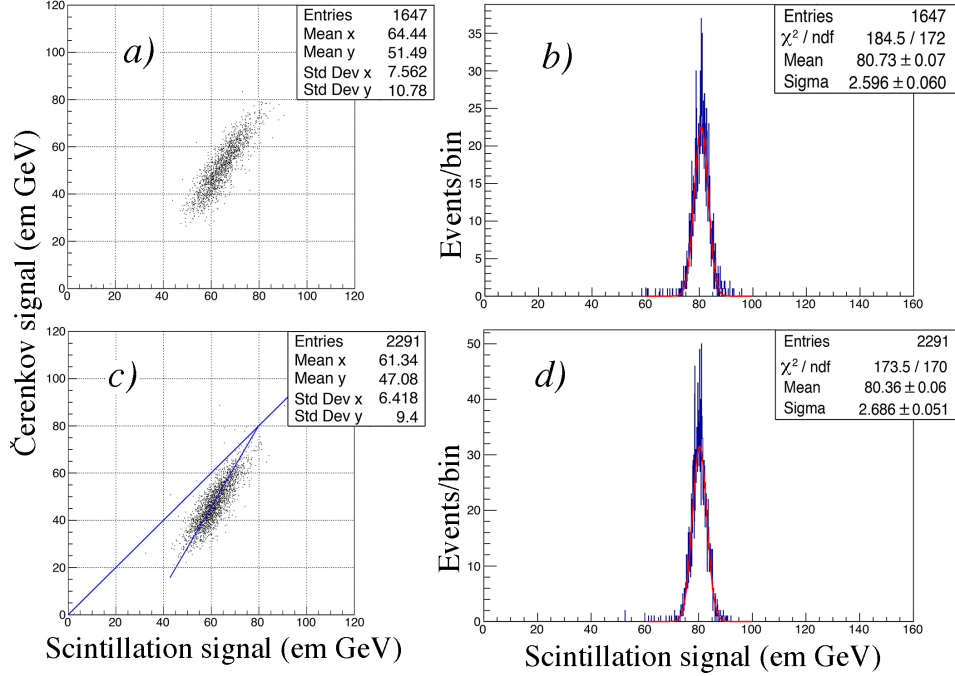
4

Figure 3: Scatter plots of the Čerenkov *vs.* the scintillation signals from showers induced by 80 GeV $\pi^+$ ($a$) and 80 GeV protons ($c$). Projection of the rotated scatter plots on the $x$ axis for the pions ($b$) and protons ($d$). The rotation procedure was identical to that used for 60 GeV $\pi^-$ (Figure 2).

+20 GeV, and found similarly good results. In addition, the use of positive polarity beams allowed us to separate the data into proton and $\pi^+$ samples. Figure 3 shows the Čerenkov *vs.* scintillation scatter plots for the 80 GeV $\pi^+$ (Figure 3a) and proton (Figure 3c) signals. These plots show a significant difference between the pion and proton signals. The average Čerenkov signal is about 10% larger for the pions than for the protons, a consequence of the absence of leading $\pi^0$s in the proton showers. However, using the intersection of the axis of the locus and the $C/S = 1$ point as the center of rotation, and the same rotation angle ($30°$) as for 60 GeV, the resulting signal distributions had about the same average value: 80.7 GeV for the pions (Figure 3b) and 80.4 GeV for the protons (Figure 3d). The widths of both distributions were also about the same: 2.60 GeV for pions, 2.69 GeV for protons. Regardless of the differences between the production of $\pi^0$s (and thus of Čerenkov light) in these two types of showers, the signal distributions obtained after the dual-readout correction procedure applied here, were thus practically indistinguishable.

We applied exactly the same procedure for the 20 GeV, 40 GeV and the 125 GeV particles, with very similar results. Also here, the average Čerenkov signals in the raw data were significantly smaller for protons than for pions. However, after applying the same rotation procedure as for the 60 and 80 GeV data (always using the same rotation angle, $\theta = 30°$), the resulting signal distributions were centered around approximately the same values, and also the relative widths of these distributions were approximately the same. The results are summarized in Table 1, which lists for each type of particle the average value of the measured Čerenkov signals, the average signal after application of the dual-readout rotation method, the fractional energy res-

5

**Table 1:** The reconstructed energy and the energy resolution for proton and pion showers, measured with the rotation method. See text for details.

| Particles | $\langle \check{\text{C}} \text{ signal}\rangle$ (em GeV) | $\langle$Reconstructed energy$\rangle$ (em GeV) | $\sigma/E$ (%) (%) | $\sigma/E \cdot \sqrt{E(\text{GeV})}$ (%) |
|---|---|---|---|---|
| 20 GeV $\pi^+$ | 8.00 | 20.5 | 6.61 | 29.5 |
| 20 GeV $p$ | 6.76 | 20.2 | 6.48 | 29.0 |
| 40 GeV $\pi^+$ | 21.7 | 41.3 | 4.49 | 28.4 |
| 40 GeV $p$ | 18.5 | 40.7 | 4.38 | 27.6 |
| 60 GeV $\pi^-$ | 38.5 | 61.0 | 3.90 | 30.2 |
| 80 GeV $\pi^+$ | 51.5 | 80.7 | 3.22 | 28.8 |
| 80 GeV $p$ | 47.1 | 80.4 | 3.34 | 29.9 |
| 125 GeV $\pi^+$ | 84.8 | 127 | 2.63 | 29.4 |
| 125 GeV $p$ | 77.8 | 126.5 | 2.85 | 31.9 |

olution ($\sigma/E$) and the fractional energy resolution multiplied with $\sqrt{E}$. All signal values are expressed in em GeV, *i.e.* the energy scale derived from the calibration with electron showers.

These results exhibit some very important features:

- The calorimeter is very linear, both for pion and for proton detection. The beam energy is correctly reconstructed at all energies within a few percent, using the energy scale for electrons, which were used to calibrate the signals.

- The reconstructed signal distributions are very narrow, narrower than those reported by any other detector we know of.

- The reconstructed signal distributions are very well described by Gaussian functions. This is illustrated in Figure 4, which shows signal distributions for hadrons at the low and high
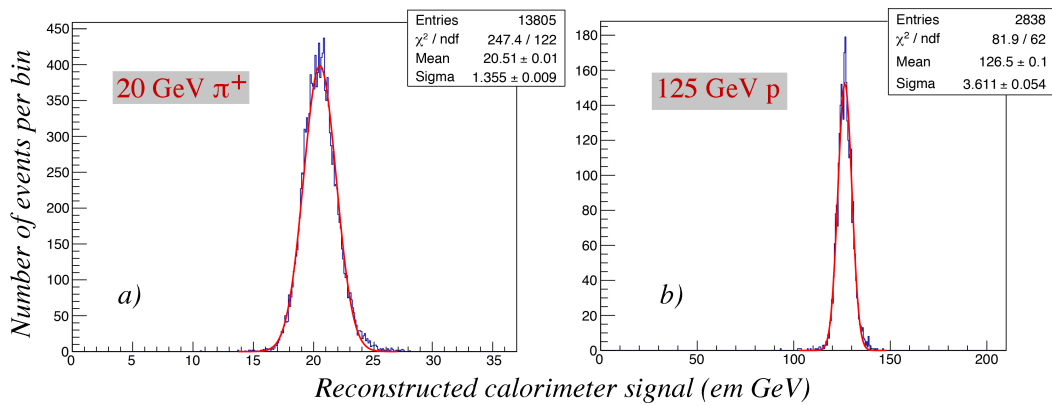


**Figure 4:** Signal distributions for 20 GeV $\pi^+$ (*a*) and 125 GeV protons (*b*) obtained with the rotation method described in the text. The energy scale is set by electrons showering in this detector.

end of the spectrum of particles studied here. The normalized $\chi^2$ values varied between 1.02 and 2.27 for all particles listed in Table 1.

- The fractional width of the reconstructed signal distribution also scales very well as expected for an energy resolution dominated by Poissonian fluctuations. Over the full energy range of 20 - 125 GeV we find: $\sigma/E = (30 \pm 2\%)/\sqrt{E}$. This result is represented by the straight line in Figure 5, which shows the experimental data points, separately for protons and pions, as a function of the beam energy.
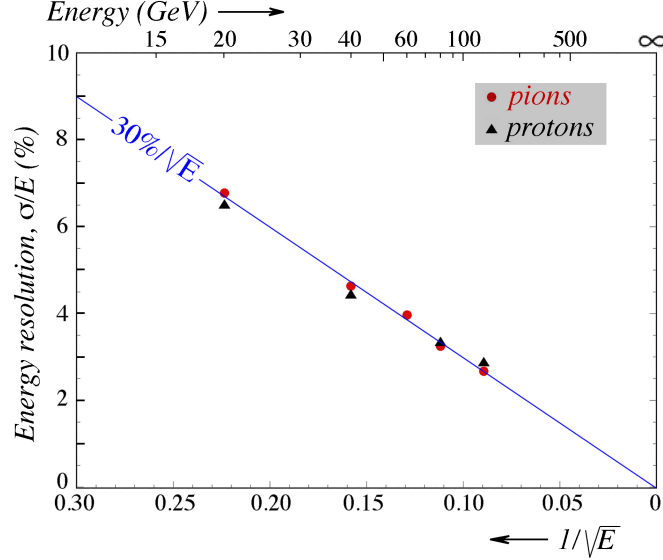


Figure 5: The fractional width of the signal distribution, $\sigma/E$, as a function of energy, for pions and protons in the 20 - 125 GeV energy range. The line represents $\sigma/E = 30\%/\sqrt{E}$.

### 2.1.3 The rotation method for multiparticle events

This method was used with the same rotation angle ($\theta = 30°$) for multiparticle events, samples of which were available for beam energies of +40, +60, +100 and +125 GeV. During these dedicated runs, the Interaction Target was installed in the beam line. Events were selected by requiring that the beam hadrons produced a signal compatible with a mip in the PSD upstream of this target and a signal of at least 6 mip in the downstream scintillation counter. No distinction was made between protons and pions for this analysis. Otherwise, the conditions were identical to the ones used for the single-hadron analysis.

Figure 6 shows an example of the signal distribution for 125 GeV multiparticle events obtained with the rotation method. This distribution shows similar features as those for single hadrons (Figure 4): A rather narrow distribution, centered at approximately the correct (energy) value, well described by a Gaussian function. However, there are also some differences, which become more obvious when we look at the results for all energies for which this analysis was carried out. These are listed in Table 2, and shown graphically in Figure 7.

7

Table 2: The reconstructed energy and the energy resolution for showers induced by pions and by multiparticle events ("jets"), measured with the rotation method. See text for details.

| Particles | $\langle \check{C}$ signal$\rangle$ (em GeV) | $\langle$Reconstructed energy$\rangle$ (em GeV) | $\sigma/E$ (%) (%) | $\sigma/E \cdot \sqrt{E(\text{GeV})}$ (%) |
|---|---|---|---|---|
| 40 GeV $\pi^+$ | 21.7 | 41.3 | 4.49 | 28.4 |
| 40 GeV "jets" | 14.7 | 37.9 | 8.32 | 52.6 |
| 60 GeV $\pi^-$ | 38.5 | 61.0 | 3.90 | 30.2 |
| 60 GeV "jets" | 27.6 | 58.0 | 6.83 | 52.9 |
| 100 GeV "jets" | 54.9 | 97.1 | 5.30 | 52.9 |
| 125 GeV $\pi^+$ | 84.8 | 127 | 2.63 | 29.4 |
| 125 GeV "jets" | 69.0 | 122.6 | 4.79 | 53.6 |

It turns out that the multiparticle signal distributions are clearly wider than those for single hadrons. However, in both cases, the fractional width scales with $E^{-1/2}$, without any significant deviations: $53\%/\sqrt{E}$ for "jets", *vs.* $30\%/\sqrt{E}$ (Figure 7b). This indicates that only stochastic fluctuations contribute to this width. The reconstructed energies are also somewhat lower in the case of the multiparticle events, more so at low energy (Figure 7a). Very substantial differences are observed in the size of the Čerenkov component, which is on average considerably smaller for the multiparticle events.

These features can be understood by realizing that the primary interaction of the beam particles took place at a distance of about 75 cm upstream of the calorimeter. Low-energy secondaries produced in these interactions may have traveled at such large angles with the beam line that they
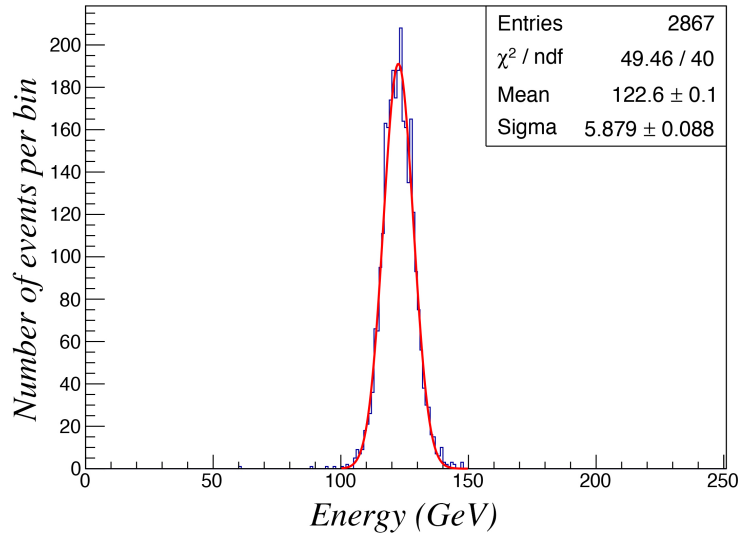


Figure 6: Signal distribution for 125 GeV multiparticle events obtained with the rotation method described in the text. The energy scale is set by electrons showering in this detector.
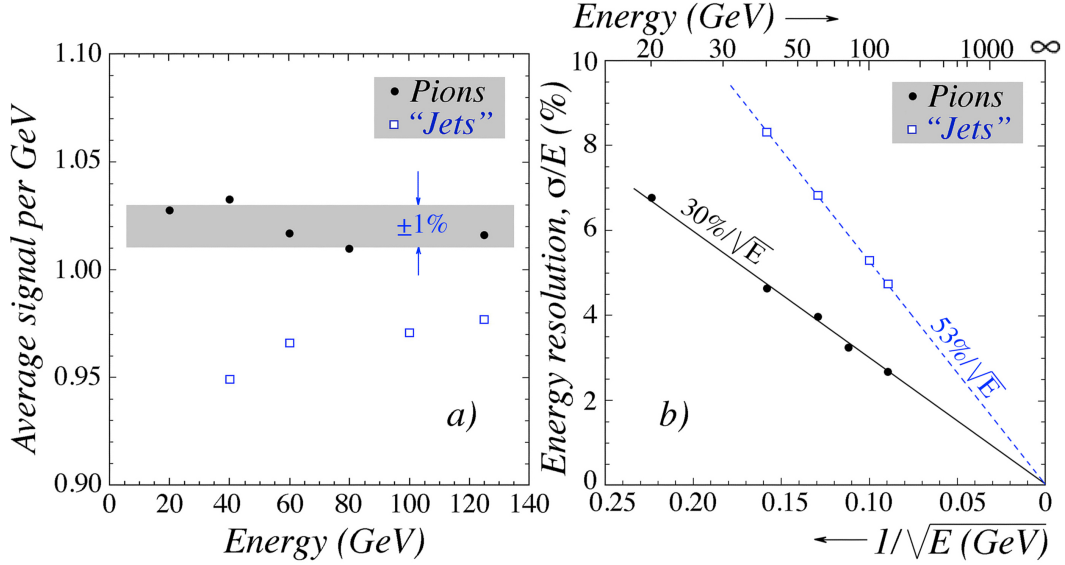
Figure 7: The average calorimeter signal per GeV (*a*) and the fractional width of the signal distribution (*b*) as a function of energy, for single pions and multiparticle events ("jets"). Results are given for the dual-readout calorimeter signals, obtained with the rotation method.

physically missed the calorimeter, as well as the leakage counters surrounding the calorimeter. The effect of that is larger when the energy of the incoming beam particle is smaller. The increased side leakage is probably also the main factor responsible for the increased width of the signal distribution. The difference in the strength of the Čerenkov component most likely reflects the fact that the average energy fraction carried by the em component in hadronic showers increases with energy. Therefore, if the energy of the incoming beam particle is split between at least six secondaries (our trigger condition for multiparticle events), the total em energy fraction is likely to be smaller than when the beam particle enters the calorimeter and deposits its entire energy there in the form of a single hadronic shower.

### 2.1.4 Discussion

Notice that we have *not* used any knowledge about the energy of the beam particles in the rotation procedure described in the previous subsections. The coordinates of the rotation center were chosen on the basis of the *equality of the hadronic Čerenkov and scintillation signals*. This implies that the hadronic response at that point must be equal to that for electrons, which was used to set the energy scale for both types of calorimeter signals. The described method has thus allowed us to measure the energy of the beam particles with great precision. The average beam energy has been correctly reproduced within a few percent for all energies studied, the fractional width of the signal distribution scaled with $E^{-1/2}$ and, most interestingly, the signal distributions were found to be essentially identical for protons and pions, despite the substantial differences between the raw scintillation and Čerenkov signal distributions for both types of particles. The latter aspect is a unique feature of dual-readout calorimetry. No other calorimeter we know of is capable of this. ATLAS has reported significant differences between the signal distributions

9

of protons and pions [6], but their "offline compensation" methods required prior knowledge of the particle type to eliminate these differences.

Yet, while we have managed to obtain very narrow signal distributions for the beam particles using only the calorimeter information, we don't think it is correct to interpret the relative width of these distributions as a measure for the precision with which the energy of an arbitrary particle absorbed in this calorimeter may be determined. The determination of the coordinates of the rotation point, and thus the energy scale of the signals, relied on the availability of an ensemble of events obtained for particles of the same energy. In practice, however, one is only dealing with *one* event and the described procedure can thus not be used in that case.
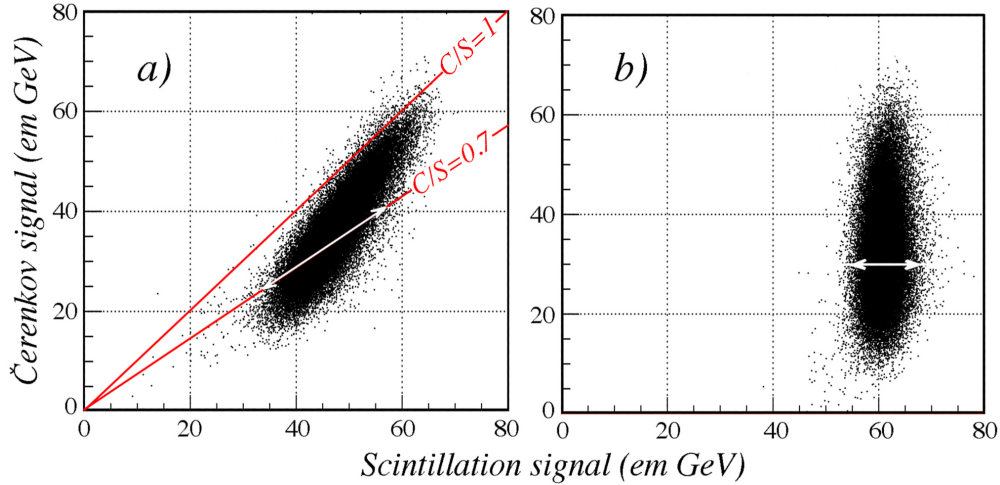


Figure 8: Scatter plots of the Čerenkov *vs.* the scintillation signals from showers induced by mono-energetic hadrons (*a*). The arrow indicates the precision with which the em shower fraction, and thus the energy, of an individual particle can be determined on the basis of the measured ratio of the Čerenkov and scintillation signals, 0.7 in this example. The rotation procedure for an ensemble of mono-energetic pions leads to the scatter plot shown in diagram *b*. The precision of the measurement of the width of that distribution is indicated by a white arrow as well.

The DREAM Collaboration has developed a procedure to determine the energy of an unknown particle showering in the dual-readout calorimeter that is *not* affected by this problem. In this procedure, described in Section 3.1, the em shower fraction ($f_{em}$) of the hadronic shower is derived from the ratio of the Čerenkov and scintillation signals. Using the known $e/h$ values of the two calorimeter structures, the measured signals can then be converted to the em energy scale ($f_{em} = 1$). The energy resolutions obtained with this method are worse than the ones given in this section, although it should be mentioned that they are dominated by incomplete shower containment and the associated leakage fluctuations, and are likely to improve considerably for detectors that are sufficiently large. However, the same is probably true for the measurements of which the results are shown in Figure 2. Figure 8 graphically illustrates the difference between the values of the energy resolution obtained with the two methods discussed here. The precision of the energy measurement is represented by the arrows in the two diagrams.

The message we want to convey in this section is that one should not confuse the precision of the energy determination of a given event based on calorimeter signals alone with the width

10

of a signal distribution obtained in a testbeam, since the latter is typically based on additional information that is not available in practice. In the example described above, this additional information derived from the fact that a large number of events generated by particles of the same energy were available. In other cases, additional information may be derived from knowledge of the particle energy. This is especially true for calorimeters whose energy scale depends on "offline compensation", or other techniques intended to minimize the total width of the signal distribution from a detector system consisting of several longitudinal segments. Such techniques rely on calibration constants whose values depend on the energy, on the type of showering particle, and sometimes also on the ratios of the signals from the different calorimeter sections.

## 2.2 First tests with SiPM readout

In October 2016, we used the few days allocated to RD52 to test our dual-readout calorimeters with a completely new type of readout: Silicon photomultipliers (SiPMs). We teamed up with a group of experts in this matter from the University of Insubria (Como), led by Professor Massimo Caccia. This type of readout offers important potential advantages for application of dual-readout calorimeters in modern experiments at colliding beam machines:

1. It offers the possibility to eliminate the forests of optical fibers that stick out at the rear end. These fiber bunches occupy precious space and act as antennas for particles that come from sources other than the showers developing in the calorimeter.

2. This compact readout makes it possible to separate the calorimeter into longitudinal segments, if so desired.

3. Unlike the PMTs we have used until now, SiPMs can operate in a magnetic field.

As a specific additional advantage for our particular type of calorimeter, we also mention the higher quantum efficiency for photon detection, which is important since fluctuations in the number of Čerenkov photoelectrons has turned out to be a limiting factor, both for the em and hadronic energy resolution. There are of course also potential disadvantages, most notably the fact that SiPMs are *digital* detectors and therefore prone to signal saturation effects. A major challenge for our particular detector concerns the fact that the SiPMs have to read the signals from a grid of closely spaced fibers of two different kinds, where the light yield of one type of fibers (detecting the Čerenkov light) is an order of magnitude smaller than that of the other fibers (detecting the scintillation light). Crosstalk was thus a major concern.

Our main goals during these first tests was the study of the mentioned crosstalk and saturation effects. Since our financial resources were extremely limited, we had to depend on off-the-shelf available components for these studies. We selected an $8 \times 8$ array of 1 mm$^2$ SiPMs, each consisting of $50 \mu m \times 50 \mu m$ pixels. This array was coupled to 64 fibers from one of our copper modules. These fibers (32 scintillating fibers and 32 Čerenkov ones) sampled the electron showers developing in a region with an effective radius of only 8.5 mm, or 0.27 $R_M$ (Moliere radius). According to EGS4 simulations of em shower development in this calorimeter, typically $\sim 50\%$ of the shower energy is deposited by an electron in this area when entering it in its center.
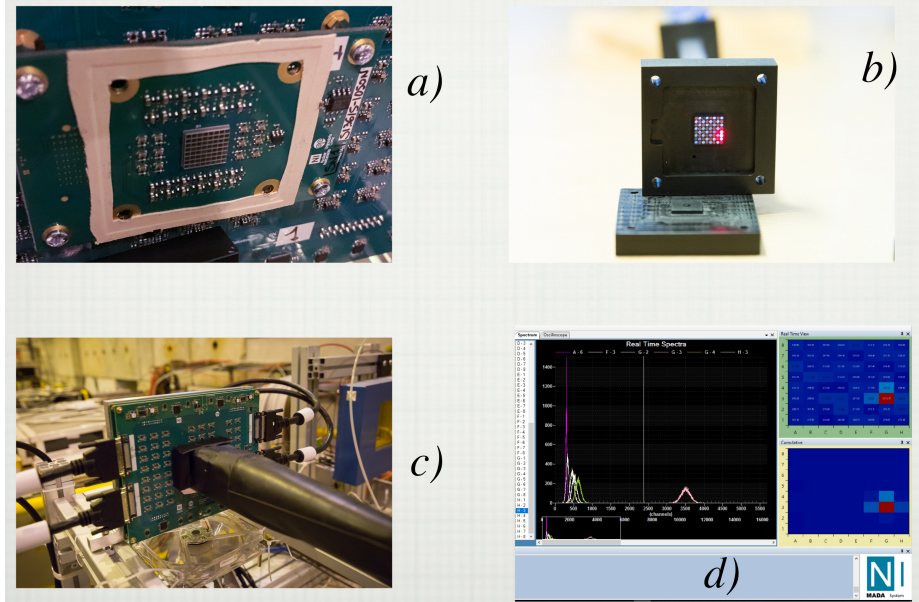
Figure 9: The 8×8 SiPM array, mounted on the electronics board (*a*) and connected to the Cu/fiber module (*c*). End view of the calorimeter module, while a narrow beam of light is sent into one of the fibers (*b*). Signals recorded in different fibers when a narrow beam of light is sent into one of the fibers. Cross talk is observed in several SiPMs connected to neighboring SiPMs (*d*).

Figure 9 shows some pictures of the SiPM array and the fiber bunch connected to it. Every fiber was connected to its own SiPM. The alignment was crucially important, as illustrated in Figure 9d, which shows the signals from light pulses injected into one particular fiber. Cross talk is observed in several SiPMs connected to neighboring SiPMs. The calibration of the SiPMs was greatly simplified by the fact that the signal distributions exhibited a structure that made it possible to count the number of photoelectrons. Figure 10 shows the distribution of the signals observed in several SiPMs in response to light signals. Such distributions made it possible to
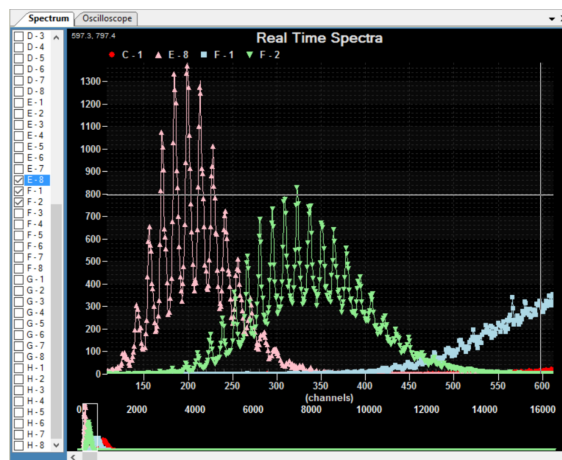


Figure 10: Signal distribution of the SiPMs in response to light signals used for calibration purposes.

establish the relationship between the signals provided by the SiPM signals and the number of individual photoelectrons (*i.e.* pixels that fired in response to the light signal). This is one of the strong points of SiPMs compared with PMTs.

The array was used to read out two different copper modules. In the first module, all 64 fibers were connected to their own individual SiPM. In the second module, only the Čerenkov fibers were connected, the scintillating fibers were retracted so that no scintillation light was detected by the SiPM array. The modules were exposed to positron beams of 20, 40, 60, 80 and 100 GeV. Figure 11 shows several event displays for 40 GeV particles. Figure 11a depicts an electron shower developing in the central region of the calorimeter, while Figure 11b shows an electron shower located slightly off-center. The event displayed in Figure 11c concerns a muon traversing the calorimeter.
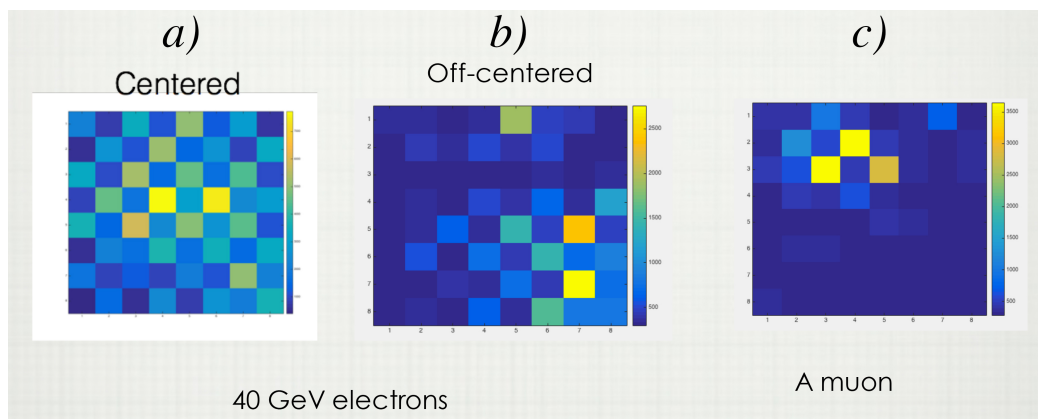


Figure 11: Event displays in the 8×8.SiPM array for a 40 GeV electron shower and a muon traversing the calorimeter. The checker board appearance of these event displays is caused by the large difference between the light yield in the scintillating and the Čerenkov fibers.

The analysis was limited to events in which the SiPM that recorded the largest signal was located in the central region of 4×4 fibers. This was an easy way to select events such as the one depicted in Figure 11a, in which the beam particles entered the calorimeter in the region covered by the SiPM readout. We should point out that each SiPM contained 400 pixels. The signals from one SiPM were thus limited to 400 photoelectrons, and saturation effects already became significant for signals consisting of less than 100 photons hitting an individual SiPM. Saturation was clearly a major issue for the S signals. Complete saturation limited the total S signals to 32×400 = 12,800 photoelectrons.

Figure 12 shows the distribution of the signals in the central four SiPMs of the array, for 40 GeV electrons. The SiPMs numbered 1 and 4 were connected to scintillating fibers, numbers 2 and 3 to Čerenkov fibers. It turned out that some of the events produced signals in SiPMs 1 and 4 that were *larger* than those expected for complete saturation, *i.e.* >400 pixels fired! We suspect that this is a manifestation of afterpulsing during the relatively long gate time (1.8$\mu$s). The figure shows that the signals in the SiPMs connected to the Čerenkov fibers were all smaller than 400 photoelectrons. However, because of the fact that the light levels in the neighboring scintillating fibers were an order of magnitude larger, it was likely that crosstalk from light produced in these neighboring fibers contributed in a major way to the Čerenkov signals.
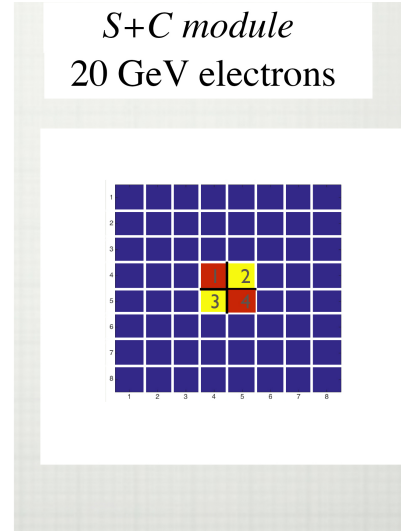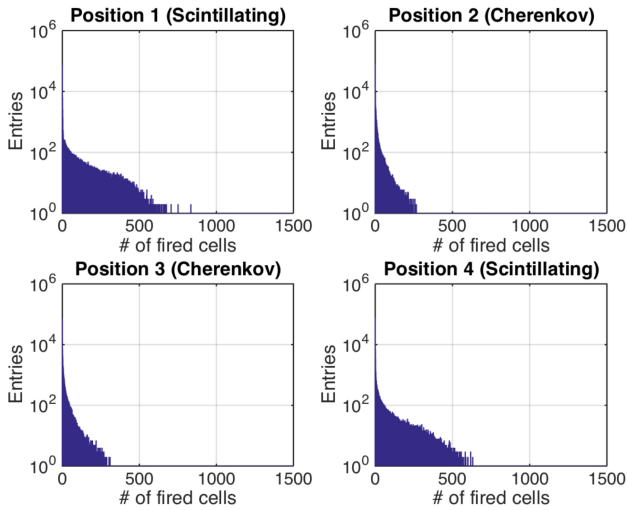
**Figure 12:** Distribution of the signals from 40 GeV electron showers measured in the central four fibers of the calorimeter in which each of the central 64 fibers was connected to its own SiPM.

Because of the saturation in the SiPMs that detected scintillation light, our main interest was focussed on the Čerenkov signals. In order to study saturation and crosstalk effects properly, we concentrated on the other calorimeter module, where *only* the Čerenkov fibers were connected to SiPMs. The scintillation light was prevented from reaching the SiPMs in this calorimeter. Signals measured in the "open" SiPMs thus were caused by Čerenkov light produced in the Čerenkov fibers, but detected somehow in the neighboring SiPMs. Figure 13 shows the distribution of the signals in the same central four SiPMs of the array, for the same 40 GeV electrons,
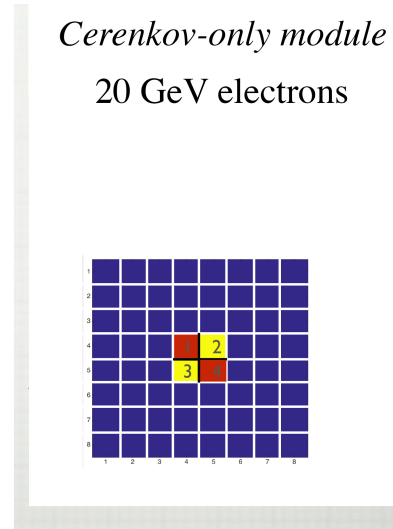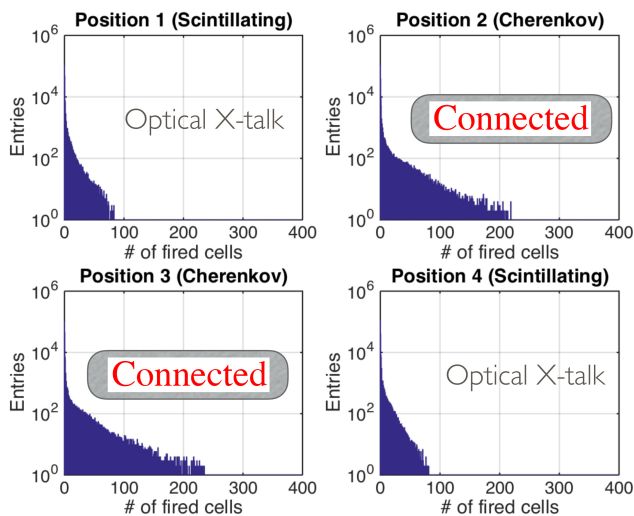


**Figure 13:** Distribution of the signals from 40 GeV electron showers measured in the central four fibers of the calorimeter in which only the 32 fibers carrying Čerenkov light were connected to the SiPMs. The other 32 SiPMs were not connected to fibers.

14

and can thus directly be compared with Figure 12. The signals in the SiPMs that are connected to the Čerenkov fibers (nrs. 2&3) are now limited to $\sim 200$ photoelectrons, well below the maximum possible level. However, at higher electron energies one should also in this case expect saturation effects. The signals in SiPMs nrs. 1&4 are an indication of the crosstalk.
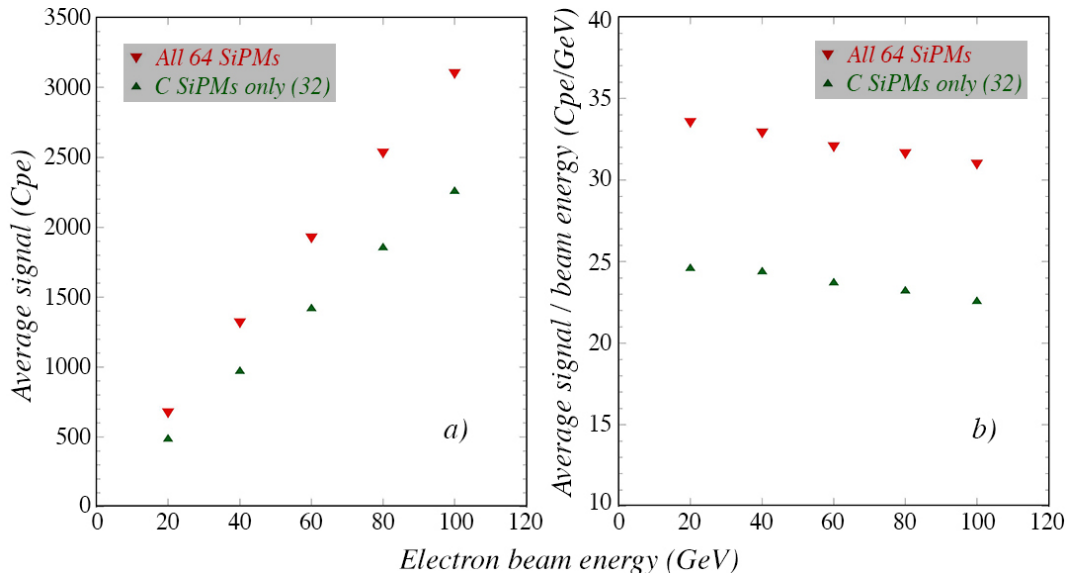


Figure 14: The average number of Čerenkov photoelectrons measured in the SiPMs as a function of the electron energy ($a$) and the average number of Čerenkov photoelectrons divided by the electron beam energy ($b$). Results are given for the calorimeter module of which *only* the clear fibers were read out by SiPMs. Results are given separately for the total signal recorded in the SiPMs to which these 32 fibers were connected, as well as the total signal in all 64 SiPMs.

In order to get a more complete idea of these effects, we looked at the *total* signals, integrated over all SiPMs, rather than those measured in individual SiPMs, and at showers from electrons at different energies. Figure 14a shows the average number of photoelectrons (*i.e.* SiPM pixels) as a function of the electron energy. The results are given separately for the total signals measured in the 32 SiPMs connected to the Čerenkov fibers, and for the total signal measured for all 64 SiPMs. A comparison between these two signal levels shows that the crosstalk was about 25%, independent of the shower energy. This number is an indication of the precision of the alignment of the fibers and the SiPMs in our setup.

Figure 14b makes it possible to assess the saturation effects. Here, the average total signals are divided by the beam energy. Also here, results are given separately for the 32 SiPMs connected to the Čerenkov fibers and for all 64 SiPMs. The figure shows a small decline with energy, as expected for saturation. The signals decrease by $\sim 8\%$ going from 20 GeV to 100 GeV. According to Figure 14a, the *average* signal in the 32 SiPMs contributing to it amounts to $\sim 70$ pixels at 100 GeV. However, one should realize that the em shower profiles are characterized by a very collimated core [7], and the observed saturation is thus very likely caused by a small number of fibers (see also Figure 13).

These data also make it possible to determine the Čerenkov light yield in this calorimeter. As mentioned earlier, the SiPM array detected about 50% of the light produced in showers from

electrons that entered the calorimeter in its center. Figure 14b indicates that the Čerenkov light yield is thus 60 - 70 photoelectrons per GeV deposited energy. This is about a factor of two more than we measured with PMT readout [7], and reflects the difference in quantum efficiency. Since this light yield is a limiting factor, both for the electromagnetic and the hadronic energy resolution achievable with this type of calorimeter, this is an important result.
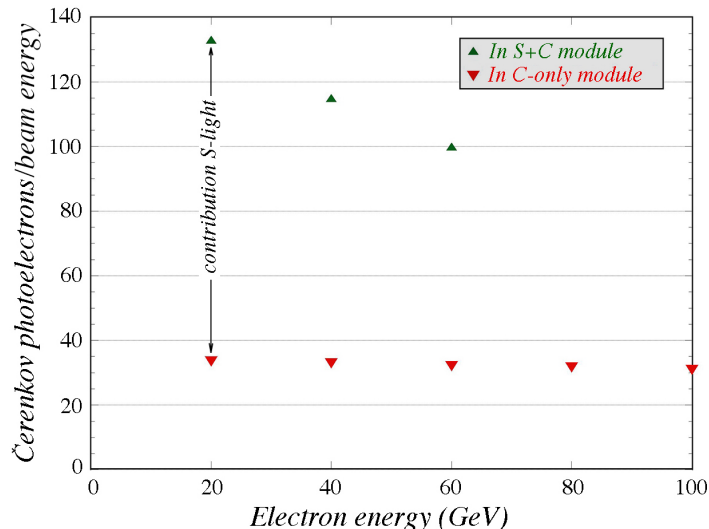


Figure 15: The average number of Čerenkov photoelectrons divided by the beam energy, as a function of the energy of the electrons. Results are given for the calorimeter module of which *only* the 32 clear fibers were read out by SiPMs, and for the calorimeter module of which *all* 64 fibers were read out .

We now come back to the results obtained with the calorimeter module of which both the Čerenkov and the scintillating fibers were connected to SiPMs. Figure 15 compares the average total signal measured by the 32 Čerenkov SiPMs in this module with the true Čerenkov signal as measured in the module where the scintillating fibers were not read out. Not surprisingly, the signals are completely dominated by the contributions of scintillation light resulting from crosstalk. This is both clear from the difference in the signals, and from the saturation effects in the Čerenkov signals, which are now very substantial. Between 20 and 60 GeV, the signal per GeV drops by 25%, while the decrease was less than 5% when only Čerenkov light contributed to the signals (Figure 14b). If we assume that also in the case of the scintillation light 25% spills over to neighboring Čerenkov SiPMs, then the difference observed at 20 GeV (a factor of 3 between the contributions of Čerenkov and scintillation light to the signals) indicates that the scintillation light yield is a factor 12 larger than the Čerenkov light yield. Taking into account the saturation effects, the real factor is probably close to 20.

# 3 Future plans

The work we have recently performed with SiPM readout was very limited in scope and was carried out with very modest resources. Given these very unfavorable boundary conditions, we feel extremely encouraged by the results. As stated in the beginning of Section 2, the possibility

to equip a dual-readout fiber calorimeter with SiPMs instead of PMTs opens up essential new application possibilities. Our work has been noticed by the people who design experiments for future colliders such as the CepC and the FCC, and the dual-readout concept has been adopted as the baseline calorimeter option by several groups. There are new funding opportunities to continue the work of the RD52 Collaboration, and build on our achievements.

Clearly, the SiPM results presented here represent a very small first step in what will probably have to be a multi-year R&D effort if one would want to bring this new approach to fruition. We have identified and quantified two fundamental issues with this new technology: Crosstalk and saturation. In the next step we propose to address these issues in more detail and work towards resolving the problems we encountered. Both issues would benefit considerably from decoupling the readout arrays for the two types of fibers. The dynamic range and the related saturation problems, which are crucial issues for the scintillation light can be alleviated by using SiPMs with smaller pixels. Hamamatsu is now offering arrays of SiPMs with $25\mu$m and even $10\mu$m pixels. That would increase the dynamic range by a factor 4 or 25, respectively, compared to the array we used last October. In the next round of experiments, scheduled for this summer, we are planning to read the signals with two independent arrays of 1 mm$^2$ SiPMs. The first array will be used to detect the signals from the scintillating fibers. The Čerenkov fibers will traverse this first array through holes at the positions where the SiPMs for these fibers were located in last year's tests, and then be read with a second array dedicated to the Čerenkov signals. In this way, the two types of signals will be completely decoupled.
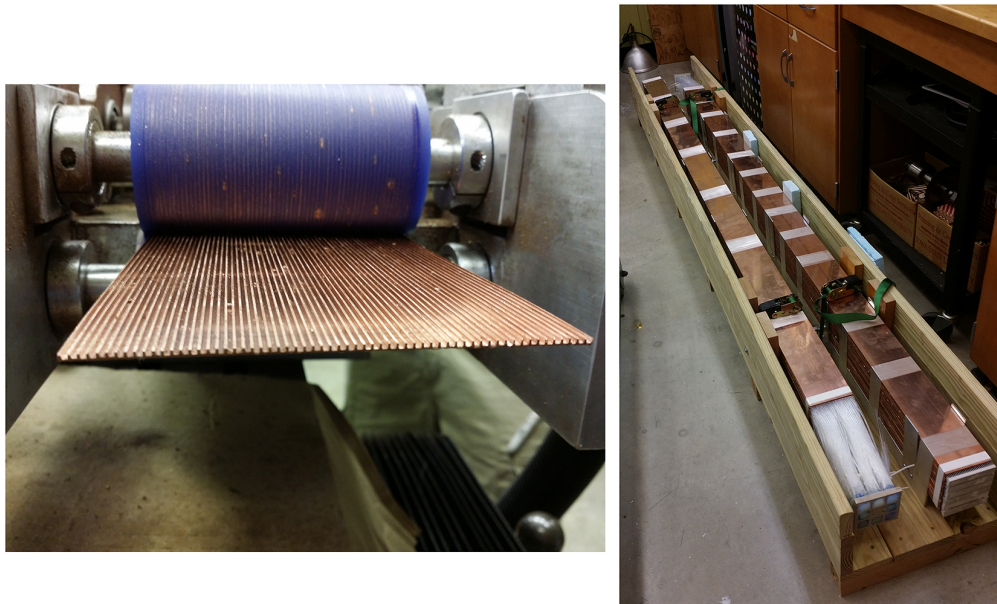


Figure 16: The new dual-readout copper modules built at Iowa State University.

In the past year, we have also made progress on another crucial issue. One of the most challenging aspects of building this type of calorimeter is the problem of how to get very large numbers of optical fibers embedded in a uniform way in the metal absorber structure. Copper, which is the most desirable absorber for dual-readout calorimetry, has turned out to be a partic-

ular difficult material to work with. Professor Hauptman, who is in charge of this component of our program, has worked tirelessly with colleagues from Kyungpook National University (Korea) and engineers of Ames Laboratory (US DoE) to find a solution for this problem, and they have produced two modules that meet the required specifications (Figure 16). We will ship these modules to CERN and plan to test them in particle beams in the H8 beam line this summer. We request the support of the SPSC for these efforts.

# References

[1] DREAM Collaboration (Wigmans R) 2010, CERN-SPSC-2010-012/SPSC-M-771.

[2] DREAM Collaboration (Wigmans R) 2016, CERN-SPSC-2016-014 ; SPSC-SR-182.

[3] N. Akchurin *et al.*, Nucl. Instr. and Meth. in Phys. Res. **A537** (2005) 537.

[4] D.E. Groom D.E., Nucl. Instr. and Meth. in Phys. Res. **572** (2007) 633.

[5] Wigmans R 2000, *Calorimetry, Energy Measurement in Particle Physics*, International Series of Monographs on Physics, Vol. 107, Oxford University Press.

[6] P. Adragna *et al.*, Nucl. Instr. and Meth. in Phys. Res. **A615** (2010) 158.

[7] N. Akchurin *et al.*, Nucl. Instr. and Meth. in Phys. Res. **A735** (2014) 130.

[8] http://highenergy.phys.ttu.edu/dream/results/publications/publications.html